A General Formulation for Simulating Physical Dispersion and a New Nine-Point Scheme

Gautam S. Shiralkar, SPE, and **Robert E. Stephenson,** SPE, Amoco Production Co.

Summary. This paper presents a general numerical formulation for simulating physical dispersion that avoids the convergence and grid-orientation problems associated with numerical dispersion. The formulation is applicable to a wide range of problems, including enhanced gasdrives with phase discontinuities. A new nine-point scheme is also presented, along with general rules for any nine-point scheme to obey Darcy's law. Converged solutions are obtained for displacements at adverse mobility ratios of 5,000 with no grid-orientation effects.

Introduction

Physical dispersion plays a critical role in determining phase behavior and recovery for many reservoir displacement processes. In miscible gasdrives, dispersion influences both sweep and displacement efficiency. Only recently, however, have attempts been made to include dispersion effects in reservoir simulators, partly because of numerical difficulties.

The straightforward inclusion of physical dispersion in conventional reservoir simulators is complicated by upstream weighting of mobilities. Upstream weighting introduces a truncation error that has a form similar to that of physical dispersion. This "numerical dispersion" cannot be related one-to-one to physical dispersion[1]; moreover, the magnitude of this numerical dispersion depends not only on grid size, but also on grid orientation, resulting in the well-known grid-orientation effect.[2] The nine-point scheme of Yanosik and McCracken[3] and other similar schemes reduce grid-orientation effects, but often do not converge as the grid is refined when upstream weighting is used.[4]

Young's[4] approach to modeling physical dispersion used centered differences for evaluating convective and dispersive fluxes. The method lacked generality, however, because it was not applicable to problems involving (a) gravity or capillary forces and (b) spatial phase discontinuities. The latter class of problems includes the important cases of enhanced gasdrives. This paper presents a general formulation for simulating physical dispersion that is not subject to these limitations.

Grid-orientation effects can be important in miscible floods with adverse mobility ratios. These require more powerful numerical schemes than traditional five-point differencing. A new nine-point scheme is presented that always gives positive transmissibilities.

Governing Equations

In the absence of dispersion, the reservoir flow of Component i is

$$\frac{\partial}{\partial t}\left(\phi \sum_{m=1}^{n_p} \rho_m S_m C_{im}\right) = \sum_{m=1}^{n_p} \nabla k \rho_m \lambda_m C_{im}(\nabla p_m - \rho_m g \nabla D). \quad (1)$$

For convenience, source/sink terms associated with wells have been omitted. In immiscible floods (e.g., waterfloods), neglecting physical dispersion is appropriate. In miscible floods, however, physical dispersion can be important, enhancing sweep efficiency and reducing displacement efficiency. To include physical dispersion, we can write

$$\frac{\partial}{\partial t}\left(\phi \sum_{m=1}^{n_p} \rho_m S_m C_{im}\right) = \sum_{m=1}^{n_p} \nabla k \rho_m \lambda_m C_{im}(\nabla p_m - \rho_m g \nabla D) + \sum_{m=1}^{n_p} \nabla K_m \rho_m \nabla C_{im}. \quad (2)$$

Bear[5] gives the following form for the dispersion tensor:

$$K_{mij} = K_{m,\text{mol}} + \alpha_{mt} |\vec{v}_m| \delta_{ij} + (\alpha_{m\ell} - \alpha_{mt}) v_{mi} v_{mj} / |v_m|, \quad (3)$$

where $i=x, y, z$ and $j=x, y, z$. Usually, molecular diffusion is negligible compared with mechanical mixing. Dispersivities $\alpha_{m\ell}$ and α_{mt} are not purely rock properties, but may depend on the flow, *viz.*, the extent of viscous fingering, saturations, and other conditions.[6] Young's approach,[4] which we follow, is to account for the primary dependence on phase velocity. For isotropic dispersion, $\alpha_{m\ell} = \alpha_{mt} = \alpha_m$, Eq. 3 simplifies to[4]

$$K_m = \alpha_m |\vec{v}_m|. \quad (4)$$

This approach may be considered a first, but important, step in including the effects of physical dispersion on a field scale. At the same time, the present work has allowed more detailed studies of laboratory-scale corefloods with a view to a better understanding and quantification of the dispersivity dependence on flow variables.

Inserting Eq. 4 into Eq. 2 gives

$$\frac{\partial}{\partial t}\left(\phi \sum_{m=1}^{n_p} \rho_m S_m C_{im}\right) = \sum_{m=1}^{n_p} \nabla k \rho_m \lambda_m C_{im}(\nabla p_m - \rho_m g \nabla D) + \sum_{m=1}^{n_p} \nabla \alpha_m |\vec{v}_m| \rho_m \nabla C_{im}. \quad (5)$$

Numerical solutions to Eq. 1 that do not introduce sufficient dispersion of some kind exhibit physically unrealistic spatial oscillations or wiggles in C_{im}.[1] These numerical wiggles represent the exact solution to the finite-difference equations.[7] The physical dispersion term in Eq. 5 eliminates the wiggles, provided that the grid size is smaller than a certain value dictated by the "maximum principle."[4]

Flows, in general, have a miscible and an immiscible aspect. We associate the convection and dispersion of concentrations with the miscible aspect. The convection term is proportional to ∇C_{im}, while the dispersion term is proportional to $\nabla^2 C_{im}$. Beyond this, any truncation error that involves $\nabla^2 C_{im}$ introduces, through a numerical scheme such as upstream weighting, an undesirable dispersion of concentrations that makes the numerical solution grid-size and grid-orientation dependent.

We associate the convection and dispersion of phase saturations with the immiscible aspect. Steep saturation gradients tend to be smeared by capillary pressure forces—e.g., in the "stabilized zone" of a waterflood front.[8] For most field-scale problems, capillary pressure effects are small enough to be unimportant. An artificial dispersion term much larger than the actual capillary pressure may then be used to avoid spatial numerical oscillations in saturation. For laboratory-scale corefloods where capillary pressure can be important, choosing a small enough grid makes the artificial dispersion negligible. The "immiscible" or "artificial" dispersion is related to $\nabla^2 S_m$ or ∇^2[function(S_m)].

Numerical Dispersion

Numerical dispersion arises from time and spatial truncation error, which introduces terms that involve $\nabla^2 C_{im}$ and/or $\nabla^2 S_m$. Peaceman[9] directly related the ratio of the numerical dispersion caused by the time truncation error to that arising from the spatial truncation error to the Courant-Friedrich-Lewy parameter $v\Delta t/\Delta x$ for certain simplified cases. In an implicit-pressure, explicit-saturation simulator like the one used here,[10] the timestep size is limited by the flow rate through each gridblock. This limitation makes the numerical dispersion from time truncation error negligible in practical cases.

The more serious numerical dispersion arises from spatial truncation error associated with the one-sided differencing of first derivatives—i.e., upstream weighting in the evaluation of convective fluxes. Although it eliminates numerical wiggles, it is not rotationally invariant; i.e., it depends on grid orientation. Although nine-point schemes reduce the grid-orientation effect, they often do not converge to a single solution as the grid is refined if upstream weighting is used.[4]

Artificial Dispersion

If a higher-order method than upstream weighting (i.e., central differencing) is used, artificial dispersion to eliminate numerical wiggles in saturation profiles must be added to the discretized flow equations. The artificial dispersion should (a) go to zero as the grid is refined—i.e., the solution should converge, (b) result in a predictable maximum principle restriction on the grid size independent of flow variables, (c) be rotationally invariant, and (d) not contribute significantly to physical dispersion—i.e., not involve $\nabla^2 C_{im}$. Also, the effect of artificial dispersion on the overall continuity equation should be minimal.

Dispersion Formulation

The approach used here is summarized as follows. Central differencing is used for all terms on the right side of Eq. 5. This second-order-correct method avoids the numerical dispersion associated with upstream weighting. Numerical wiggles in C_{im} are eliminated by the physical dispersion term, provided that the grid size is smaller than dictated by the maximum principle. Similarly, elimination of numerical wiggles in S_m requires introduction of an artificial dispersion term.

Young's formulation[4] could not handle gravity or capillary pressure effects because it inherently equated fractional-phase flow with fractional-phase mobility. The artificial dispersion term he proposed could also yield spurious physical dispersion over and above that desired through the introduction of a $\nabla^2 C_{im}$ term even for single-phase flow.[11]

A more general formulation is presented below, which is constructed to allow for both gravity and capillary pressure.

$$\frac{\partial}{\partial t}\left(\phi \sum_{m=1}^{n_p} \rho_m S_m C_{im}\right)=\nabla \sum_{m=1}^{n_p} \frac{\rho_m (k_r)_t}{\mu_m} k_{rfm} C_{im} k \nabla \Phi_m$$

$$+ \sum_{m=1}^{n_p} \nabla \alpha_a k |\nabla \Phi_m| \frac{\rho_m}{\mu_m} (k_r)_t \nabla (k_{rfm} C_{im})$$

$$+\nabla \sum_{m=1}^{n_p} (\alpha_m - \alpha_a) k |\nabla \Phi_m| \frac{\rho_m}{\mu_m} (k_r)_t k_{rfm} \nabla C_{im}, \quad \ldots\ldots (6)$$

where $(k_r)_t = \sum_{m=1}^{n_p} k_{rm}$, ... (7a)

$$k_{rfm} = k_{rm}/(k_r)_t, \quad \ldots\ldots (7b)$$

and $\alpha_a = \max(\Delta x/2,\ \Delta y/2,\ \Delta z/2)$. ..... (8)

When the last two terms of Eq. 6 are combined, the amount of physical dispersion, d_{phy}, is

$$d_{\text{phy}} = \nabla \sum_{m=1}^{n_p} \alpha_m k |\nabla \Phi_m| \frac{\rho_m}{\mu_m} (k_r)_t k_{rfm} \nabla C_{im}$$

$$= \nabla \sum_{m=1}^{n_p} \alpha_m |\vec{v}_m| \rho_m \nabla C_{im} \quad \ldots\ldots (9)$$

and the amount of artificial dispersion, d_{art}, is

$$d_{\text{art}} = \nabla \alpha_a \sum_{m=1}^{n_p} k |\nabla \Phi_m| \frac{\rho_m}{\mu_m} (k_r)_t C_{im} \nabla k_{rfm}. \quad \ldots\ldots (10)$$

Because our formulation does not equate fractional mobility with fractional flow, both gravity and capillary pressure effects can be handled. Also, because k_{rfm} is a function of S_m and not of C_{im}, d_{art} does not directly introduce any spurious physical dispersion. Thus, the impact of d_{art} on the miscible aspect of flow, where physical dispersion effects are important, is minimized. The effect of d_{art} on the overall continuity equation is

$$\sum_{i=1}^{n_c} \nabla \alpha_a \sum_{m=1}^{n_p} k |\nabla \Phi_m| \frac{\rho_m}{\mu_m} (k_r)_t C_{im} \nabla k_{rfm}$$

$$= \nabla \alpha_a (k_r)_t \sum_{m=1}^{n_p} k |\nabla \Phi_m| \frac{\rho_m}{\mu_m} \nabla k_{rfm}. \quad \ldots\ldots (11)$$

This term is not identically zero, but because the artificial dispersion flux is computed along the gradient of the fractional relative permeability, the effect on the overall continuity equation is minimized. By contrast, the immiscible part of the numerical dispersion introduced by upstream weighting occurs along a gradient of the unscaled quantity $(\rho_m \lambda_m)$, and the effect on the overall continuity equation is larger, especially for cases with large gradients in density and/or mobility.

The grid-size restriction arising from the maximum principle is

$$\max(\Delta x, \Delta y, \Delta z) \le \min(2\alpha_m). \quad \ldots\ldots (12)$$

An example simulation presented in Fig. 9 of Ref. 11 at $N_{\text{Pe}}=72.5$ requires a 37×37 grid (a 39×39 grid was actually used). Eq. 12 places a practical limitation for high N_{Pe} for larger field studies.

Phase-Discontinuity Problem

When a phase exists in one gridblock but not in the next, a difficulty arises in evaluation of the ∇C_{im} terms because molar fractions are undefined for the missing phase. In a recent paper,[12] this problem was circumvented by the use of values for the molar fractions in the missing phase equal to those projected from an adjacent two-phase node. However, the method was reported to suffer from restrictive stability limitations.

A new algorithm is illustrated in **Fig. 1**. Without loss of generality, we consider the case of a discontinuous gas phase. Gridblock P contains both oil and gas. Its neighboring gridblock E contains oil but no gas—i.e., $V_E=0$.

The mole balance for Component i may be written

$$y_i = \frac{z_i - (1-V)x_i}{V}, \quad \ldots\ldots (13)$$

so that $\nabla y_i = (1/V)[\nabla z_i - (1-V)\nabla x_i + x_i \nabla V]$

$$-(\nabla V/V^2)[z_i - (1-V)x_i]. \quad \ldots\ldots (14)$$

Evaluating this at the blocks' midpoint (for central differencing) gives

$$\nabla y_i \cong (1/\bar{V})[\nabla z_i - (1-\bar{V})\nabla x_i + \bar{x}_i \nabla V]$$

$$-(\nabla V/\bar{V}^2)[\bar{z}_i - (1-\bar{V})\bar{x}_i], \quad \ldots\ldots (15)$$

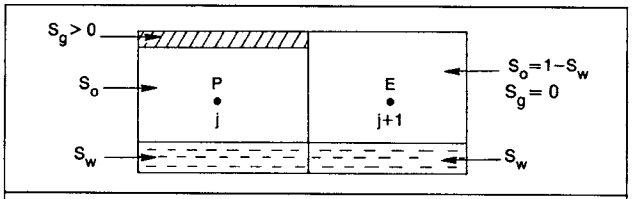

Fig. 1—Phase discontinuity between gridblocks.

where $\bar{V}=(V_E+V_P)/2$, ...(16a)

$\bar{z}_i=[(z_i)_E+(z_i)_P]/2$, ...(16b)

and $\bar{x}_i=[(x_i)_E+(x_i)_P]/2$. .....(16c)

Thus, the algorithm works by formulating the flux in terms of variables x_i, z_i, and V, which are defined in both nodes, rather than in terms of y_i, which is undefined at Node E.

We recognize the limitations of this approach. At a phase discontinuity, Eqs. 1 and 5 cannot be integrated across the discontinuity without invoking some sort of jump condition, which can be obtained only by a proper consideration of the physical processes occurring locally at the interface. This is beyond the scope of the present paper. The approach presented above is thus a method designed to overcome a numerical problem. The formulation is not sensitive to grid size or grid orientation.

When a gridblock connection experiences a loss in phase continuity we switch from Eq. 6 to the following:

$$\frac{\partial}{\partial t}\left(\phi \sum_{m=1}^{n_p} \rho_m S_m C_{im}\right)=\nabla \sum_{m=1}^{n_p} k(\rho_m\lambda_m)_t C_{im}\lambda_{fm\rho}\nabla\Phi_m + \sum_{m=1}^{n_p} \nabla\alpha_a|k\nabla\Phi_m|(\rho_m\lambda_m)_t\nabla(\lambda_{fm\rho}C_{im}) + \sum_{m=1}^{n_p} \nabla(\alpha_m-\alpha_a)|k\nabla\Phi_m|(\rho_m\lambda_m)_t\lambda_{fm\rho}\nabla C_{im}, \quad \text{.....(17)}$$

where $(\rho_m\lambda_m)_t = \sum_{m=1}^{n_p} \rho_m\lambda_m$ .....(18)

and $\lambda_{fm\rho}=(\rho_m\lambda_m)/(\rho_m\lambda_m)_t$. .....(19)

For the node without Phase m, $\lambda_{fm\rho}=0$ and $(\lambda_{fm\rho}C_{im})=0$ (the bulk flow capacity of a missing phase is zero) and all terms in Eq. 17 are evaluated by use of central differences. The last term is evaluated with the expression for ∇C_{im} developed earlier in Eqs. 15 and 16.

New Nine-Point Scheme

Although the dispersion formulation presented above is rotationally invariant, we have found that for highly adverse mobility ratios, a nine-point method gives converged results with minimal grid-orientation effects at a coarser grid than a five-point scheme. **Fig. 2** shows recovery curves obtained in a 2D areal simulation of secondary (no mobile water) -contact-miscible displacement in a five-spot for $M=40$ and $N_{Pe}=39.4$. Comparison of apparently converged results obtained with a five-point scheme and a diagonal grid on one hand and a parallel grid on the other indicate a small difference in recovery owing to grid orientation. Better agreement could possibly be achieved if the grids are refined even further. A nine-point formulation, discussed below, achieves better results with a much coarser grid.

The Yanosik-McCracken nine-point scheme[3] does not consider anisotropy and can yield negative transmissibilities for heterogeneous systems, resulting in severe stability problems. Other nine-point schemes we examined either gave negative transmissibilities or were not always consistent with Darcy's law.[13] Here we present a new nine-point scheme that always yields positive transmissibilities and is consistent with Darcy's law.

Although the discussion focuses on transmissibilities, similar weightings are used to compute dispersion fluxes. Consider an element shown in **Fig. 3** of size $\Delta x\times\Delta y$ with diagonal transmissibilities T_{14} and T_{23} and edge transmissibilities T_{12}, T_{34}, T_{13}, and T_{24}. While the diagonals represent their full values, the edge transmissibilities are one-sided; i.e., in considering flow from Node 2 to 1, the total transmissibility is the sum of the one-sided edge transmissibilities from two elements adjoining at the Interface 1/2, shown dotted in Fig. 3.

Consider a 1D flow in the x direction such that $(p_1-p_3)=(p_2-p_4)=\Delta p$, $p_1=p_2$, and $p_3=p_4$. Darcy's law applied across the element yields

$$(\overline{k_xh})\Delta y\Delta p/\Delta x=(T_{13}+T_{24}+T_{14}+T_{23})\Delta p, \quad \text{.....(20)}$$

where $\overline{k_xh}$ is some average of nodal k_xh values—e.g.,

$$\overline{k_xh}=[(k_xh)_1+(k_xh)_2+(k_xh)_3+(k_xh)_4]/4, \quad \text{.....(21)}$$

so that $T_{13}+T_{24}+T_{14}+T_{23}=(\overline{k_xh})\Delta y/\Delta x=q_x$. .....(22)

Eq. 22 states that the sum of the x-directional edge transmissibilities plus the sum of the diagonal transmissibilities must equal the total element x-directional conductance, q_x, for any nine-point scheme. Similarly,

$$T_{12}+T_{34}+T_{14}+T_{23}=(\overline{k_yh})\Delta x/\Delta y=q_y. \quad \text{.....(23)}$$

We also require that the pressure difference, Δp, applied along a principal axis of permeability (x axis) will not produce a flow in the orthogonal, y, direction—i.e.,

$$T_{23}\Delta p-T_{14}\Delta p=0, \quad \text{.....(24)}$$

so that $T_{23}=T_{14}$. .....(25)

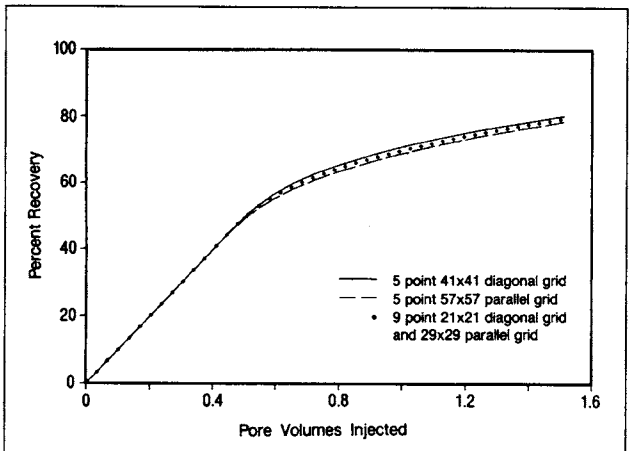

Fig. 2—Recovery for 2D areal secondary-contact miscible displacement, five- and nine-point results, $M=40$.

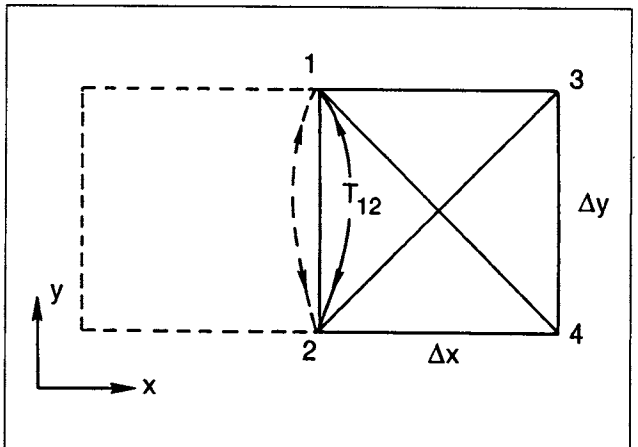

Fig. 3—Four-node element used to derive nine-point transmissibilities.

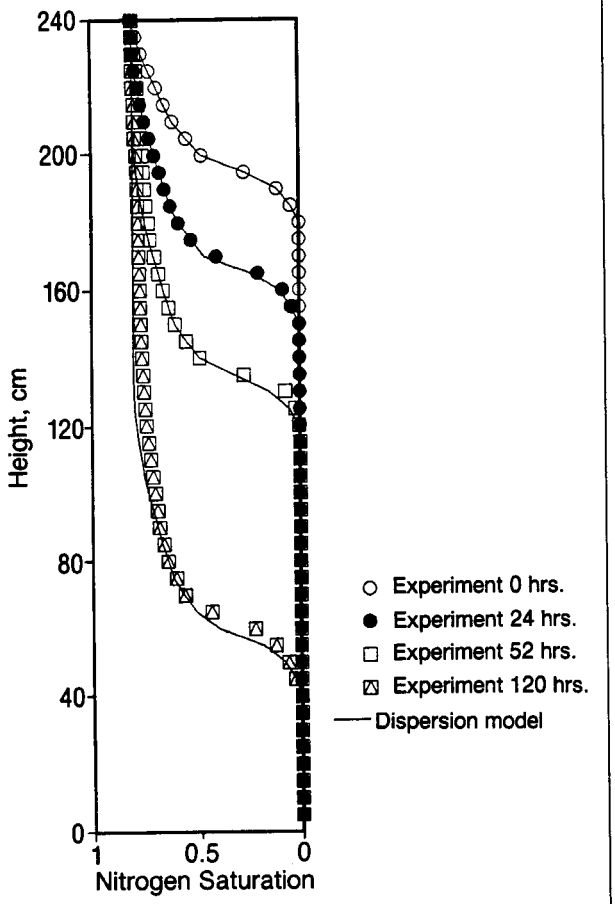

Fig. 4—Comparison of predicted nitrogen saturation profile with Terwilliger *et al.*[8] gravity-drainage experiment; displacement rate is 0.101 cm³/min.

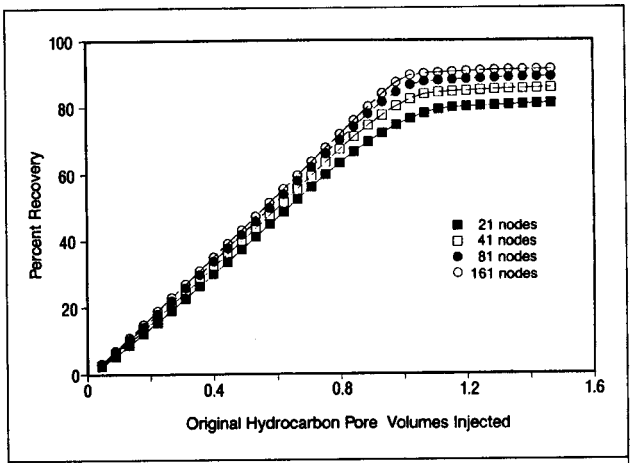

Fig. 5—Recovery for 1D secondary enhanced gasdrive displacement, upstream weighting.

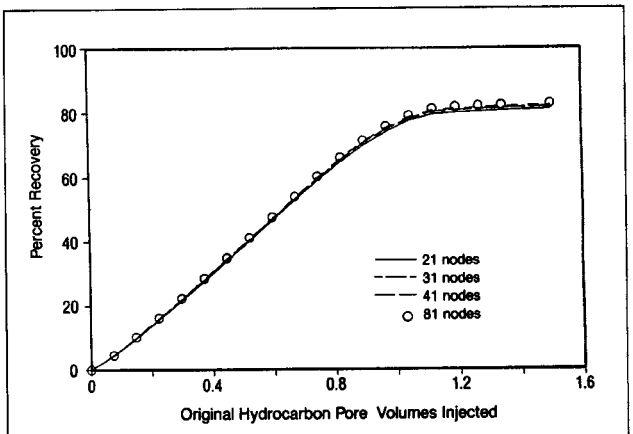

Fig. 6—Recovery of 1D secondary enhanced gasdrive displacement, dispersion model, $N_{Pe}=40$.

Eq. 25 implies that for a nine-point scheme, the diagonal transmissibilities must be equal. Otherwise, a pressure gradient along a principal axis of permeability will induce flow in an orthogonal direction. Several nine-point schemes we examined violated this condition.[13]

Our numerical experiments indicate that the optimum weighting for a square grid ($\Delta x=\Delta y$) in a homogeneous, isotropic system is when

$$T_{14}=T_{23}=\tfrac{1}{2}(T_{12})=\tfrac{1}{2}(T_{34})=\tfrac{1}{2}(T_{13})=\tfrac{1}{2}(T_{24})=q_x/6=q_y/6. \quad \ldots\ldots\ldots\ldots\ldots\ldots\ldots\ldots\ldots\ldots (26)$$

Therefore, we also require this weighting under the given conditions.

We use Eq. 27 to define the diagonal transmissibilities:

$$T_{14}=T_{23}=\tfrac{1}{3}[q_xq_y/(q_x+q_y)]. \quad \ldots\ldots\ldots\ldots\ldots\ldots\ldots\ldots\ldots\ldots (27)$$

Because a nine-point formulation represents (in a sense) a weighted average of the equations for a grid system (e.g., diagonal grid) and a rotated grid system (e.g., parallel grid), it is the diagonal transmissibilities that are a measure of the relative weighting of the rotated grid system. In the new nine-point scheme, we ensure positive transmissibilities by apportioning the remaining x conductance $[q_x-(T_{14}+T_{23})]$, which is always positive, between T_{13} and T_{24} on the basis of permeabilities—i.e.,

$$(T_x)_{edge}=q_x-(T_{14}+T_{23}), \quad \ldots\ldots\ldots\ldots\ldots\ldots\ldots\ldots\ldots\ldots (28)$$

$$T_{13}=\frac{(k_xh)_1+(k_xh)_3}{4(\overline{k_xh})}(T_x)_{edge}, \quad \ldots\ldots\ldots\ldots\ldots\ldots\ldots\ldots\ldots\ldots (29)$$

and $T_{24}=(T_x)_{edge}-T_{13}$. $\ldots\ldots\ldots\ldots\ldots\ldots\ldots\ldots\ldots\ldots (30)$

Transmissibilities T_{12} and T_{34} are defined similarly. Note that all transmissibilities calculated by the new nine-point scheme will be positive, a requirement for model stability.

Behavior of New Nine-Point Scheme

We now discuss the behavior of our nine-point scheme with various heterogeneities, anisotropies, and grid aspect ratios. For the base case of a square grid in a homogeneous, isotropic system, the new nine-point scheme gives the optimum weighting of Eq. 26.

In a square grid in an isotropic ($k_x=k_y$) but heterogeneous system (nonuniform k_x), the new nine-point scheme gives diagonal transmissibilities equal to those of the Yanosik-McCracken nine-point formulation, but unlike the latter, the edge values are always positive.

For a homogeneous, isotropic system with $\Delta y/\Delta x\neq 1$, the new nine-point scheme reduces to the Yanosik-McCracken formulation identically.

Finally, we consider the case of a homogeneous but anisotropic system—i.e., uniform k_x and uniform k_y but $k_x\neq k_y$. The anisotropic problem can be converted to an equivalent isotropic problem under a coordinate transformation:

$$x'=(k/k_x)^{1/2}x=(k_y/k_x)^{1/4}x, \quad \ldots\ldots\ldots\ldots\ldots\ldots\ldots\ldots\ldots\ldots (31)$$

$$y'=(k/k_y)^{1/2}y=(k_x/k_y)^{1/4}y, \quad \ldots\ldots\ldots\ldots\ldots\ldots\ldots\ldots\ldots\ldots (32)$$

$$k=(k_xk_y)^{1/2}, \quad \ldots\ldots\ldots\ldots\ldots\ldots\ldots\ldots\ldots\ldots (33)$$

and $$\frac{\partial}{\partial x}\left(k_x\frac{\partial p}{\partial x}\right)+\frac{\partial}{\partial y}\left(k_y\frac{\partial p}{\partial y}\right)=k\left(\frac{\partial^2 p}{\partial x'^2}+\frac{\partial^2 p}{\partial y'^2}\right). \quad \ldots\ldots\ldots\ldots (34)$$

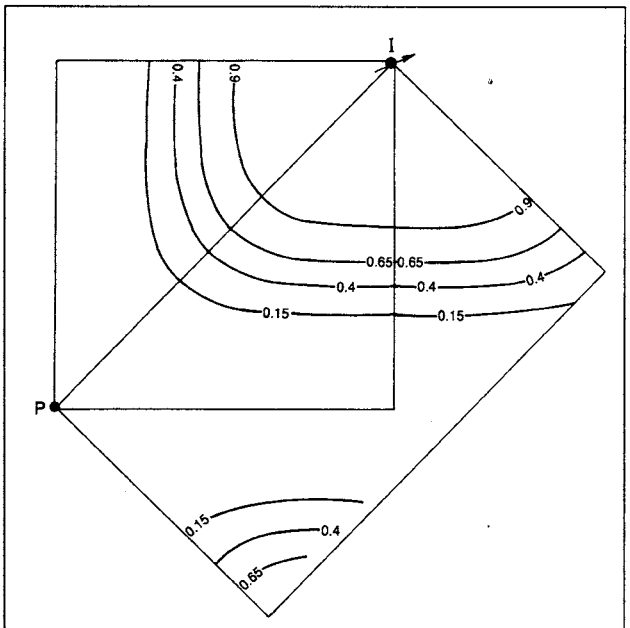

Fig. 7—Solvent concentration at 0.36 PV injected for 2D areal secondary-contact-miscible displacement, $M=5{,}000$ and $N_{Pe}=28$.

If we apply the new nine-point scheme to the anisotropic problem, we obtain

$$T_{14}=T_{23}=\tfrac{1}{3}\frac{q_x q_y}{q_x+q_y}=\tfrac{1}{3}\frac{k_x k_y}{k_x(\Delta y/\Delta x)+k_y(\Delta x/\Delta y)}$$

$$=\tfrac{1}{3}\frac{(k_x k_y)^{1/2}\Delta x'\Delta y'}{(\Delta x'^2+\Delta y'^2)}, \quad \ldots\ldots\ldots\ldots\ldots\ldots\ldots\ldots\ldots\ldots (35)$$

where $\Delta x'=(k_y/k_x)^{1/4}\Delta x$ ..... (36a)

and $\Delta y'=(k_x/k_y)^{1/4}\Delta y$. ..... (36b)

This is equivalent to transforming the anisotropic problem with k_x, k_y, Δx, and Δy into an equivalent isotropic problem with $k=(k_x k_y)^{1/2}$ and a transformed grid $\Delta x'$, $\Delta y'$ and then using the Yanosik-McCracken formula. This is also true for the edge values. Thus, for this case, the new nine-point scheme represents a logical extension of the Yanosik-McCracken formula to anisotropic systems.

The new nine-point scheme has proved successful in simulations that also used conventional upstream weighting. Here, however, we present only results pertaining to the dispersion formulation.

Example Problems

The dispersion formulation and new nine-point scheme were incorporated into an existing generalized compositional simulator.[10] Some highlights of the testing program are presented here. **Fig. 4** shows the nitrogen saturation profile predicted in modeling the Terwilliger *et al.*[8] experiments. Brine was displaced vertically downward through a tube packed with unconsolidated sand by nitrogen under pressure at a rate of 0.101 cm³/minute and saturation profiles measured. The simulation used the capillary pressure curves and other properties reported in Ref. 8. A successful match was obtained. This problem is dominated by gravity and capillary pressure effects.

Fig. 5 shows the extreme sensitivity to grid size of the predicted recovery when upstream weighting is used to simulate a 1D enhanced gasdrive displacement of a synthetic oil containing methane, n-butane, and decane under secondary initial conditions (connate water). Pure methane is injected at 2,500 psia and 160°F. A modified Redlich-Kwong equation of state (EOS) was used to compute fluid properties. **Fig. 6** shows that, unlike upstream weighting, the

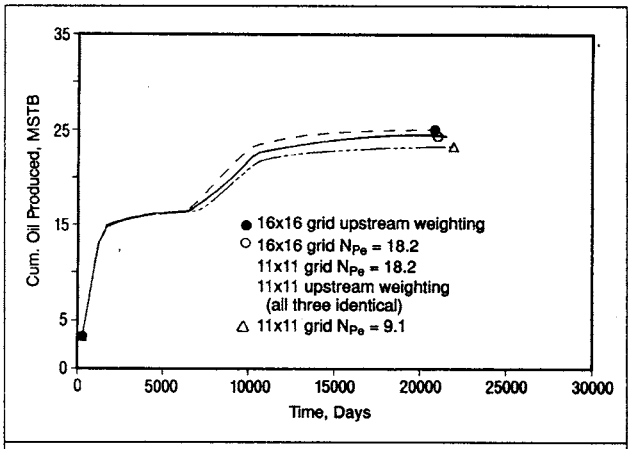

Fig. 8—2D areal simulation of secondary through tertiary recovery in a quarter of a five-spot pattern.

recovery is much less sensitive to grid size when the dispersion formulation is used. Problem parameter details are given in Table 1 of Ref. 11. This problem, which involves spatial phase discontinuities, shows the insensitivity to grid size of our method.

Fig. 7 shows injected-solvent-concentration contours for an areal, equal-density, constant-rate, contact-miscible displacement with no water present for $M=5{,}000$ and $N_{Pe}=28$. Contours for both parallel-grid and diagonal-grid simulations are shown. For convenience, the entire parallel grid (half of a five-spot) has not been shown but only the section directly overlying the diagonal grid (quarter of a five-spot) and extending some distance beyond. Fig. 8 of Ref. 11 showed corresponding recovery curves, indicating lack of sensitivity to grid size (convergence) and grid orientation. $M=5{,}000$ was chosen to demonstrate the numerical power of the dispersion formulation when used in conjunction with the new nine-point scheme.

In Fig. 9 of Ref. 11, the predicted recovery for secondary-contact miscible displacement in a quarter of a five-spot at $M=40$ ($N_{Pe}=72.5$) was shown to agree well with the experimental recovery curve published by Habermann[14] at $M=38.2$, in agreement with Young.[12]

Fig. 8 shows oil recovery for a quarter of a five-spot simulation. Injection of one original HCPV of water is followed by a water-alternating-gas (WAG) process during which a 20% original HCPV slug of solvent is injected with an equal volume of water over 10 cycles. This is followed by 15 cycles of WAG during which a 30% original HCPV slug of chase gas is injected with an equal volume of water. Finally, 0.5 original HCPV of chase water is injected. A modified Redlich-Kwong EOS was used with a nine-component characterization of the hydrocarbon fluids. Further details of the problem parameters are presented in Table 2 of Ref. 11. Results for 11×11 and 16×16 grids are shown in Fig. 8, indicating that a converged solution was obtained. Also shown are two equivalent upstream-weighted simulations. Note that these are not converged. Fig. 8 also shows that halving N_{Pe} (doubling the physical dispersion) decreases ultimate recovery. As with the 1D case, the method proposed in this paper to overcome the phase-discontinuity problem works well for a 2D case.

Conclusions

1. A general formulation for simulating the effects of physical dispersion for complex and practical problems was presented. It is applicable to a wide class of problems, including those with gravity and capillary forces and phase discontinuities.
2. The formulation is not sensitive to grid orientation or grid size.
3. A new nine-point method was developed that always yields positive weightings, which is important for model stability. It has been used to simulate high-adverse-mobility-ratio displacements ($M=5{,}000$) with minimal sensitivity to grid size and grid orientation.
4. The dispersion formulation and the new nine-point scheme lend themselves readily to incorporation into existing reservoir simulators.

Authors


Shiralkar

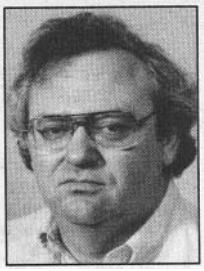
Stephenson

Gautam S. Shiralkar is a staff research engineer in the reservoir engineering section at Amoco Production Co. in Tulsa. He was previously with Sohio Petroleum Co. and earlier worked for General Electric in thermal hydraulics. He holds a BTech degree from the Indian Inst. of Technology, an MS degree from the Massachusetts Inst. of Technology, and a PhD degree from the U. of California, Berkeley, all in mechanical engineering. Robert E. Stephenson, research supervisor, joined Amoco in 1978. He has worked in reservoir model development, EOR simulations, and reservoir engineering workstations. He holds a BS degree from the Indiana Inst. of Technology, an MS degree from Brigham Young U., and a PhD degree from Clemson U., all in chemical engineering.

5. In example problems, we matched published experimental data, showed that the dispersion formulation and new nine-point scheme give converged solutions, demonstrated that very-high-mobility-ratio displacements can be simulated, and showed the effects of dispersion on recovery of a WAG process.

Nomenclature

C = concentration
d_{art} = artificial dispersion
d_{phy} = physical dispersion
D = depth
g = acceleration of gravity
h = height
k = permeability
k_r = relative permeability
k_{rfm} = fractional relative permeability of Phase m
K = effective dispersion coefficient
L = system length, equal to half-pattern spacing for five-spot
M = mobility ratio
n_c = total number of components
n_p = total number of phases
N_{Pe} = Peclet number$=L/\alpha$
p = pressure
q = conductance (flow capacity)
S = saturation
t = time
T = transmissibility
v = velocity
V = vapor mass fraction
x,y = Cartesian coordinates
x_i = oleic molar fraction of i
$\Delta x,\Delta y$ = grid interval
y_i = vapor molar fraction of i
z_i = overall molar fraction of i
α = physical dispersivity
α_a = artificial dispersivity
$\alpha_{m\ell}$ = longitudinal dispersivity of Phase m
α_{mt} = transverse dispersivity of Phase m
λ = mobility$=k_r/\mu$
λ_{fm} = fractional mobility of Phase m
$\lambda_{fm\rho}$ = fractional mass mobility ($\rho\lambda$) for Phase m
μ = viscosity
ρ = density
ϕ = porosity
Φ = phase potential

Subscripts

g = gas
i = Component i
m = phase
mol = molecular
o = oil
t = total
w = water

Acknowledgment

Permission to publish this work was granted by Amoco Production Co.

References

1. Russell, T.F. and Wheeler, M.F.: "Finite Element and Finite Difference Methods for Continuous Flows in Porous Media," *Mathematics of Reservoir Simulation*, R.E. Ewing (ed.), SIAM, Philadelphia (1983) 67.
2. Todd, M.R., O'Dell, P.M., and Hirasaki, G.J.: "Methods for Increased Accuracy in Numerical Simulation," *SPEJ* (Dec. 1972) 515–30.
3. Yanosik, J.L. and McCracken, T.A.: "A Nine-Point, Finite-Difference Reservoir Simulator for Realistic Prediction of Adverse-Mobility-Ratio Displacements," *SPEJ* (Aug. 1979) 253–62; *Trans.*, AIME, **257**.
4. Young, L.C.: "A Study of Spatial Approximations for Simulating Fluid Displacement in Petroleum Reservoirs," *Computer Methods in Applied Mechanics & Engineering* (Dec. 1984) 3–46.
5. Bear, J.: *Dynamics of Fluids in Porous Media*, American Elsevier, New York City (1972) 613.
6. Salter, S.J. and Mohanty, K.K.: "Multiphase Flow in Porous Media: I. Macroscopic Observations and Modeling," paper SPE 11017 presented at the 1982 SPE Annual Technical Conference and Exhibition, New Orleans, Sept. 26–29.
7. Roache, P.J.: *Computational Fluid Dynamics*, Hermosa Publishers, Albuquerque, NM (1976) 161.
8. Terwilliger, P.L. *et al.*: "An Experimental and Theoretical Investigation of Gravity Drainage Performance," *Trans.*, AIME (1951) **192**, 285–95.
9. Peaceman, D.W.: *Fundamentals of Numerical Reservoir Simulation*, Elsevier Scientific Publishing Co., New York City (1977) 68–74.
10. Young, L.C. and Stephenson, R.E.: "A Generalized Compositional Approach for Reservoir Simulation," *SPEJ* (Oct. 1983) 727–42.
11. Shiralkar, G.S. and Stephenson, R.E.: "A General Formulation for Simulating Physical Dispersion and a New Nine-Point Scheme," paper SPE 16975 presented at the 1987 SPE Annual Technical Conference and Exhibition, Dallas, Sept. 27–30.
12. Young, L.C.: "The Use of Dispersion Relationships To Model Adverse-Mobility-Ratio Miscible Displacements," *SPERE* (Aug. 1990) 309–16.
13. Coats, K.H. and Modine, A.D.: "A Consistent Method for Calculating Transmissibilities in Nine-Point Difference Equations," paper SPE 12248 presented at the 1983 SPE Symposium on Reservoir Simulation, San Francisco, Nov. 15–18.
14. Habermann, B.: "The Efficiencies of Miscible Displacement as a Function of Mobility Ratio," *Trans.*, AIME (1960) **219**, 264–73.

SI Metric Conversion Factors

bbl	× 1.589 873	E−01	= m^3
°F	(°F−32)/1.8		= °C
in.	× 2.54*	E+00	= cm
psi	× 6.894 757	E+00	= kPa

*Conversion factor is exact.

SPERE

Original SPE manuscript received for review Sept. 27, 1987. Paper accepted for publication July 25, 1990. Revised manuscript received May 3, 1990. Paper (SPE 16975) first presented at the 1987 SPE Annual Technical Conference and Exhibition held in Dallas, Sept. 27–30.